Molecular relaxation in a photosensitive liquid-crystalline polymeric glass former

1999 J. Phys.: Condens. Matter 11 A355

(http://iopscience.iop.org/0953-8984/11/10A/032)

J. Phys.: Condens. Matter **11** (1999) A355–A362. Printed in the UK PII: S0953-8984(99)00063-6

Molecular relaxation in a photosensitive liquid-crystalline polymeric glass former

L Cristofolini, P Facci, P Camorani and M P Fontana

Dipartimento di Fisica and Istituto Nazionale di Fisica della Materia, Università degli Studi di Parma, via delle Scienze, I-43100 Parma, Italy

Received 2 October 1998

Abstract. We have measured the relaxation to equilibrium in the supercooled nematic phase upon approach to T_g of a fragile liquid-crystalline photosensitive polymeric glass former. Perturbation is introduced in a non-conventional way by optical pumping (orientation) of the nematic polydomain phase. Relaxation back to equilibrium is followed both on the microscopic scale, by means of depolarized time-resolved Raman experiments, and on the macroscopic scale, by means of quartz crystal microgravimetry.

1. Introduction

An interesting aspect of the glass transition in supercooled fluids is the role of cooperativity and space non-homogeneities [1]. Due to their molecular complexity, polymers yield fragile, non-homogeneous glassy phases. Recently much work was performed on photosensitive side-chain polymers, mostly because of their potential applications as high-density optical memories, optical switches, non-linear devices, etc. Particularly interesting are the liquid-crystalline side-chain polymers (LCP) [2], in which cooperativity is enhanced by the mesogenic interactions of the side-chain moiety. In these materials the complexity of the system and its interactions yields structural and dynamical inhomogeneities on a wide range of length and time scales. In particular, absorption of light in the UV–visible spectral range leads to molecular reorientation, variations in the index of refraction anisotropy, domain formation and reorientation, and variations in the internal stress distribution.

The most important and studied optical perturbation mechanism is photoinduced *trans–cis* isomerization in the side chain [3], which is generally made up of an azobenzene moiety attached to the main polymeric chain via a polymethylenic flexible spacer. The mesogenic azobenzene, upon illumination in the violet–UV range, undergoes *trans–cis* isomerization, which takes place on the nanosecond timescale and the nanometre length scale. Due to the strong molecular anisotropy in the *trans*-configuration, the molecular transition dipole moment will be essentially parallel to the main molecular axis; hence selective pumping with linearly polarized light will change the molecular orientational distribution, eventually reorienting the molecules in the plane perpendicular to the polarization of the pump light [4]. Such an effect will depend on the pump power density, wavelength, and polarization. Thus the orientational distribution function of the side chains can be altered with remarkable flexibility. This process has measurable effects on all space scales: at the molecular level, the already-mentioned change in the orientational distribution of the single molecules; mesoscopically, the optical pump will alter the domain morphology and index of refraction anisotropy. Macroscopically, we expect

0953-8984/99/SA0355+08$19.50

such changes to influence the viscoelastic behaviour, or the internal stress distribution due to interdomain interaction effects.

Optical pumping has another important effect: the *trans*-form (planar, small electric dipole moment) is mesogenic, whereas the *cis*-form (non-planar, larger dipole moment) is not. If, due to optical pumping, the number of *cis*-molecules reaches a threshold level (typically a few per cent of the total), the liquid-crystalline (e.g. nematic) phase is 'poisoned', i.e. the system undergoes an isothermal phase transition to an isotropic phase [5]. Thus the mesogenic potential of the system can be externally controlled, yielding other possibly useful optical effects.

The combined action of external optical perturbation, nematic interactions, and polymeric main-chain conformational dynamics make this a very complex system, which however can be useful in the study of the role of space and time non-homogeneities and cooperativity in the relaxation behaviour of the overcooled fluid upon approach to the glass transition, when the system is taken out of equilibrium by optical pumping. In particular, it may be of interest that all of the effects originate in the microscopic isomerization process, then propagate to the mesoscopic and macroscopic scale through the mesogenic interaction and the permanence effects of the polymeric network.

In this paper we wish to focus mainly on the relaxation of optically induced spatial inhomogeneities following molecular reorientation due to optical pumping, using in a somewhat unconventional manner two techniques, namely fluctuation micro-Raman spectroscopy (FRS), which should probe the relaxation of the molecular orientational distribution over sample areas as small as a few square microns, and quartz crystal micro-gravimetry (QCM), which is used here as a sensitive macroscopic probe of internal stress relaxation, due in our case to the rearrangement of domains.

2. Experimental techniques

The specific material that we studied is PA4: poly[[4-pentiloxy-3′-methyl-4′-(6-acryloxy-exyloxy)]azobenzene] [6]; it shows solid–nematic and nematic–isotropic transitions at 83 °C and 96 °C respectively upon heating. The nematic phase strongly undercools directly into a fragile glassy phase with $T_g = 21$ °C [7]. Thin layers of this material were prepared by cast solution in chloroform, for thicknesses of 1–5 μm, or by Langmuir–Blodgett deposition, for thicknesses of up to 0.4 μm.

Raman scattering yields information on vibrational and reorientational dynamics and relaxation on the microscopic (picoseconds, nanometre) scale, and on local symmetry and ordering. In particular, FRS probes the time autocorrelation function of molecular reorientational fluctuations [8]. What is measured are the polarized and depolarized spectral band shapes of appropriate vibrational modes of a simple molecule or molecular subgroup in a complex molecule (this is the case that we shall consider here). The spectral integral of such a Raman line is related to the $t = 0$ limit of the correlation function, i.e. to the reorientational static structure factor $R(q)$. Since the light wavelength is much larger than molecular dimensions, R is probed in the $q \approx 0$ limit. Thus the depolarization ratio of an appropriate Raman line is sensitive to the molecular symmetry (and hence local order) and the long-range orientational order, and their eventual changes. This is the substance of the so-called VV–VH experiment, where VV and VH refer to the polarized and depolarized integral intensities respectively. Such an experiment can also yield information on reorientational dynamics through Fourier band-shape analysis of the VV–VH components. This yields directly the orientational time correlation function in the time range of about 0.5 to 5 ps.

In anisotropic fluids such as liquid crystals, R is related to the orientational distribution

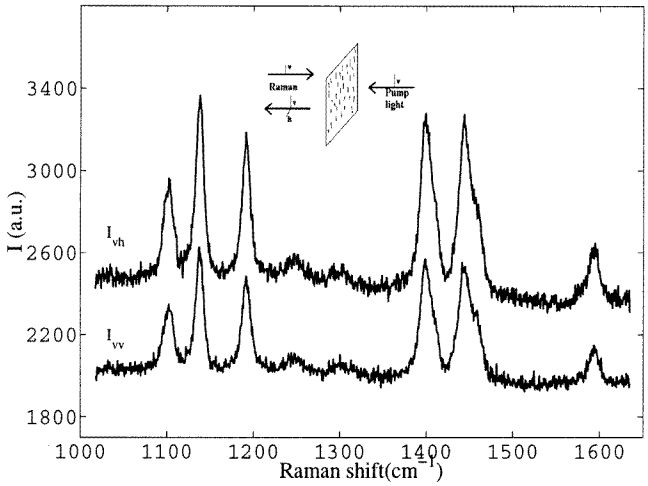

Figure 1. Raman spectra collected in the VV (bottom trace) and VH (top trace) geometries at $T = 50\ ^{\circ}$C. The integration time is 30 s in each case. The geometry of the Raman experiment is sketched in the inset.

function, whose second and fourth moments S_2 and S_4 (e.g. the order parameters) can be determined by measuring the depolarization ratios $R_1 = I_{zy}/I_{zz}$, $R_2 = I_{yz}/I_{yy}$, and $R_3 = I_{xy}/I_{xx}$ of a totally symmetric vibration in an oriented monodomain sample [9]. In the back-scattering geometry, the nematic axis is directed along z; R_1 and R_2 refer to planar alignment, and R_3 to homeotropic alignment. Light propagates along x in the first two cases and along z in the third case (see the inset in figure 1).

The dynamic VV–VH experiment can also be performed on low-molecular-weight liquid crystals [10]; however, for complex materials such as LCPs such an experiment is very difficult, and we have obtained only very qualitative results.

If the molecular orientational distribution is altered by some external perturbation, then R, and hence also R_i ($i = 1, 2, 3$), will acquire time dependence. In particular, after the perturbation is turned off, $R(t)$ will reflect the return to equilibrium of an appropriate orientational correlator $f_{R(t)}$, which can be determined by following any of the R_i.

Preliminary measurements by means of FRS and photoinduced birefringence (PIR) [11] showed that at least part of the dynamics of the molecular system's return to equilibrium takes place over long timescales (seconds to hours).

Because of this, we were able to use FRS in a time-resolved mode, and hence determine the time-dependent $f_{R(t)}$ on this long timescale. This is made possible by an important characteristic of side-chain LCPs, due to the interplay between the side-chain nematic potential on the one hand and the conformational dynamics of the main chain on the other.

FRS data were taken in back-scattering geometry with a micro-Raman spectrometer equipped with a LN_2-cooled CCD detector. The typical spot size was of the order of a few μm^2. The sample thickness was typically about 1 μm (0.4 μm for the Langmuir–Blodgett multilayers). With such thicknesses, the FRS data are free from polarization-scrambling effects.

We could obtain an acceptable signal-to-noise ratio for our depolarization ratio measurements with an integration time of 15 s. This allowed us to follow R_i over time with a resolution of below one minute. The spectra were taken with polarized 633 nm light at <5 mW cm^{-2} power density. Of the several peaks due to the azobenzene side chain, we

selected the mode at 1139 cm^{-1} (the benzene ring C–H in-plane deformation). Although R_i is the ratio between the depolarized (VH) and polarized (VV) components, most of the time changes concerned the VH part, which is the one that we discuss here; we have performed control measurements by recording also the VV component to obtain R, but the results were the same. Optical pumping was provided by a polarized (V or H) 458 nm argon laser beam at power densities ranging from <1 mW cm^{-2} to over 500 mW cm^{-2}. In this paper we shall report the data obtained at 10 mW cm^{-2}. A more complete report, which will include the power density and wavelength dependence of the effects, is in preparation [12].

Changes in the index of refraction anisotropy were followed using PIR also in a pump probe configuration; here for brevity we shall not discuss these data in detail (see [11, 12]).

The viscoelastic relaxation following optical pumping was measured using a relatively novel technique, namely quartz crystal microgravimetry (QCM) [13]. The resonance frequency of a quartz crystal is not only sensitive to the amount of mass deposited on it, but also to the interface boundary and the stress, for a solid film, or viscoelastic properties, for a highly viscous fluid. Thus such characteristics can be followed easily and simply by monitoring the resonance frequency over time. Clearly in this case the signal yields information averaged over the whole sample. In our case the unperturbed frequency was 10 MHz, and we could determine its changes with a 1 Hz resolution. For further details we refer the reader again to our forthcoming paper [12].

3. Results and discussion

Before presenting and discussing our data, it may be useful to recall that there are two distinct regions in the photoinduced phase diagram of our sample [11]: for a given power density on the sample, there exists a temperature T_p such that for $T > T_p$, the nematic phase is poisoned, and the sample is in the isotropic phase. Thus there is no long-range nematic order, is no birefringency, and are no domains: this is confirmed by our PIR data [12]. When the optical pump is turned off, the *cis–trans* isomerization process will eventually reduce the number of *cis*-molecules below the threshold necessary to frustrate the nematic potential, and the sample will revert to the nematic phase, with a relaxation time which will depend both on the *cis–trans* isomerization process and on the processes of domain formation in the presence of the slowing-down effects due to the main chain.

For $T < T_p$, however, the photoinduced *cis*-molecules are not present in sufficient number to frustrate the nematic potential; the sample is in a nematic phase, and the dominant effect of the optical pump is the reorientation of the side chains. In the pump phase we deal with the imposition of a non-equilibrium distribution of molecular orientations, which can be described in terms of an *effective* order parameter connected to a pseudo-nematic axis. Both in value and in orientation such quantities are wholly determined by the external perturbation, as long as $T < T_p$. The pump process thus leads to an effectively monodomain pseudo-nematic phase. When the pump is turned off, the monodomain structure reverts back to the equilibrium polydomain morphology of an ordinary nematic phase.

Thus, although the *trans–cis* isomerization process is the microscopic basis of the optical pumping process and of the poisoning effect on the nematic phase, the processes that we probe are predominantly connected to intra- or interdomain relaxation.

In figure 1 we show typical Raman spectra collected on PA4 in the VV (bottom trace) and VH (top trace) geometries at $T = 50\ ^{\circ}$C just after the pump light orientation process has been carried out. The subsequent intensity analysis is performed on the peak at 1139 cm^{-1}, which is a totally symmetric vibration of C–H in the benzene ring. Its degree of polarization directly provides us with information about the orientation of the azobenzene side-chain group. As

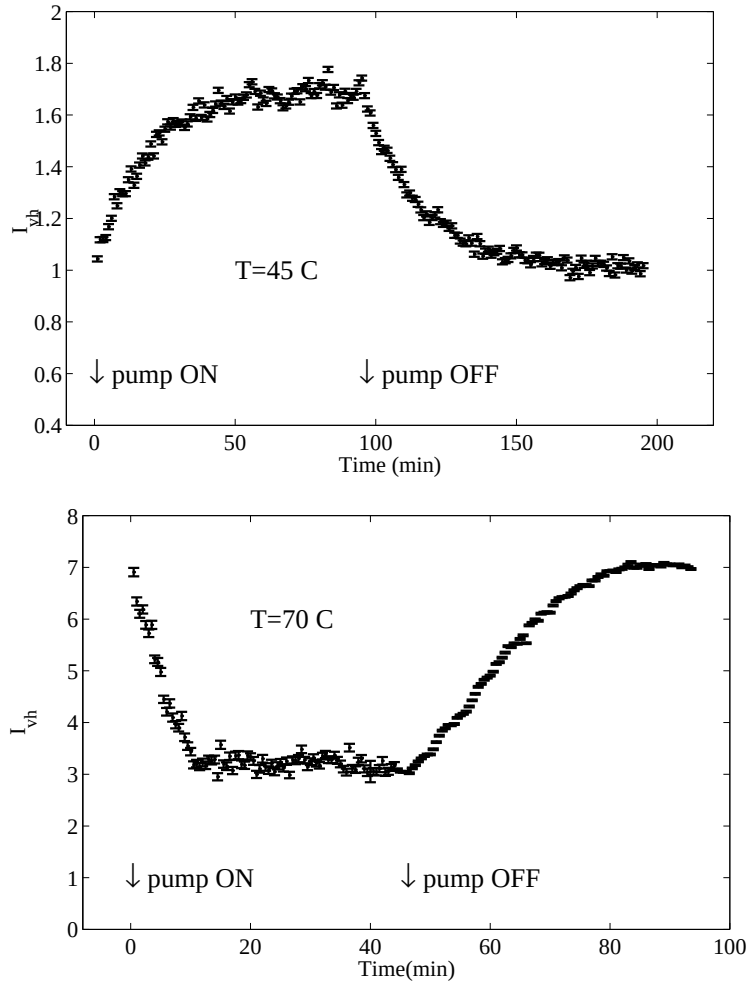

Figure 2. The time dependence of the intensity of the Raman peak at 1139 cm^{-1} in the VH configuration at $T = 45\,^{\circ}C$ (top panel) and $T = 70\,^{\circ}C$ (bottom panel). The arrows mark the times at which the pump laser was switched on and off.

already mentioned, we follow the depolarization ratio $R_2 = I_{yz}/I_{yy} = I_{VH}/I_{VV}$, where z is the direction of the photoinduced pseudo-nematic director, which in the case of vertically polarized pump light lies is the horizontal direction H, and y is the vertical axis V. In the polydomain 'virgin' nematic phase prior to optical alignment, $R_2 = 1$ due to the disorder of the nematic directors in the area probed by the Raman spot. As alignment is photoinduced, a single horizontal pseudo-nematic domain is formed; consequently R_2 grows to its saturation value $R_2 \approx 2$ which corresponds to an effective order parameter $S_2' \approx 0.7$. When the pump light is switched off, the pseudo-monodomain slowly relaxes to a polydomain. We follow this change through the time evolution of the intensity I_{VH} in the VH configuration.

In figure 2, top panel, we show I_{VH} as a function of time during and after optical pumping at $T = 45\,^{\circ}C$. The arrows mark the times at which the pump light is switched on and off. Both the pump and the relaxation portions of the cycle follow, within the rather large error limits of our experiment, a simple exponential law, with the same value for τ: 21 ± 2 min. We found

that the relaxation back to equilibrium follows a simple exponential law for $T > 26$ °C and a Kohlrausch–Williams–Watts (KWW) stretched exponential at lower temperatures. In the bottom panel of figure 2 we show the same process for $T > T_p$. Under the action of the optical pump, the depolarized Raman intensity decreases to the value typical of the isotropic phase. Switching off the pump light restores the nematic phase with a dynamics which is initially related to the *cis–trans* molecular isomerization process only, and then predominantly to the nematic domain formation processes.

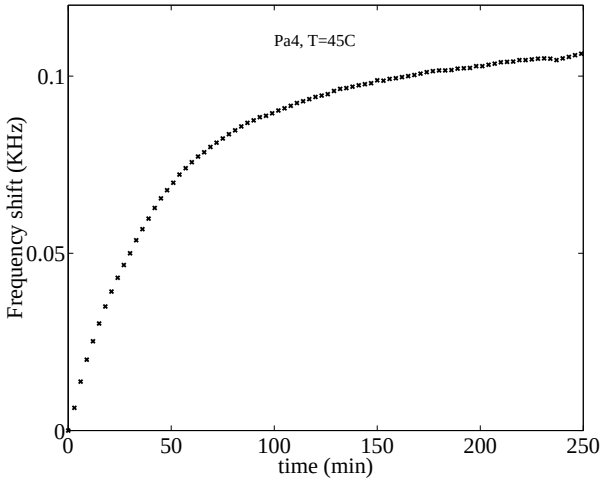

Figure 3. The time dependence of the viscoelastic relaxation ($T = 45$ °C) following optical pumping, as probed by the frequency shift measured by the QCM technique.

In figure 3 we show the interdomain stress relaxation after pumping. Although the process seems to be again following a simple exponential, the overall values of τ were almost a factor of 5 longer at all temperatures.

In figure 4 we compare the two sets of data for τ as measured by the micro-balance and

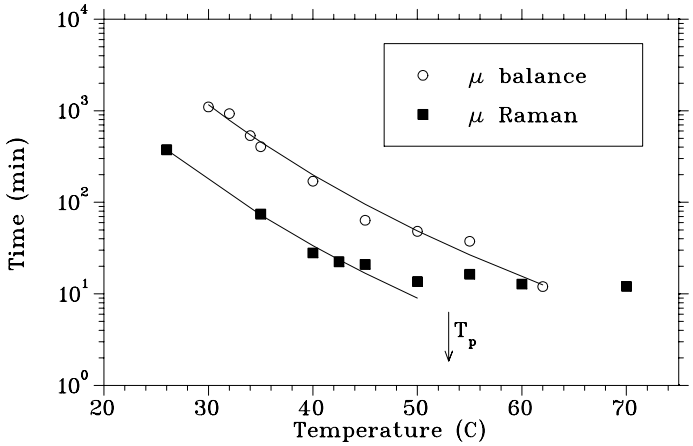

Figure 4. Symbols: the T-dependence of the relaxation times (minutes) returning to equilibrium measured by the QCM (open circles) and micro-Raman (filled squares) techniques. The continuous lines are the VFT fits described in the text. The vertical arrow marks the poisoning temperature T_p.

the Raman techniques. We note that, despite the already-mentioned difference of a factor of 5 between results obtained by the two techniques, in the T-range up to T_p the temperature dependences of τ are the same. The solid lines in figure 4 are Vogel–Fulcher–Tammann (VFT) fits:

$$\tau(T) = \tau_0 \exp\left(\frac{T_a}{T - T_0}\right)$$

to the data (up to T_p for the micro-Raman technique; over the whole T-range for the QCM technique).

The deviation from the VFT fit of the Raman data for $T > T_p$ is clearly due to the different weights of the relaxation processes to which the Raman probe is sensitive below and above T_p. Such a difference does not apply to the QCM probe, which is sensitive at all temperatures to the interdomain stress-relaxation effects. The fact that the temperature dependence of the relaxation time τ probed by FRS changes above T_p and that it reaches the same value as that for the QCM at $T = 70\ ^\circ$C may well be a mere coincidence, but it can also be indicative of a crossover between different relaxation channels taking place at that temperature. Further work is needed to elucidate this point.

We found the best fit in figure 4 by fixing the activation temperature to the value measured by dynamical mechanical analysis (DMA) ($T_a = 1270$ K [14]), thus obtaining values for T_0 (220 ± 20 K for both Raman and QCM techniques) consistent with the value obtained by DMA ($T_0 = 243 \pm 3$ K [14]). The different values for τ_0 which are obtained ($\tau_0 = 40 \pm 5\ \mu$s for the Raman technique; $\tau_0 = 150 \pm 20\ \mu$s for the QCM technique) reflect the different mechanisms probed.

4. Conclusions

Our most important finding is the strong similarity in the relaxation behaviours probed with two very different techniques: FRS and QCM. In both cases we found a good fit of the temperature dependence of the relaxation times with the same T_0. We note that our value for T_0 is very close to the one determined by DMA techniques.

Another interesting point concerns the question of the orientational correlator probed by depolarized FRS. In the classic three-geometries experiment [9], the system is at equilibrium and the results yield the values of the scalar order parameters S_2 and S_4. In our case we perturb the vector part of the orientational distribution: the scalar order parameters may also be affected (as is indeed the case for the experiments at $T > T_p$) but this is not necessary to produce the effects that we observe at lower temperatures. In fact, a perusal of the typical variation of S_2 and S_4 over the whole nematic phase shows that the variations in R_i due to the scalar part of the molecular ordering would give a small contribution to the observed variation of R_i following optical pumping. Therefore the orientational correlator probed by our experiment involves the fluctuations of the pseudo-nematic axis. That such fluctuations are characterized by such a slow dynamics is a feature which warrants further investigation. However, it is very probably a manifestation of the coupling between the orientations of the side chains and the conformations of the main chain.

References

[1] Hansen J-P, Levesque D and Zinn-Justin J (ed) 1991 *Liquids, Freezing and Glass Transition* (Amsterdam: North-Holland)

Donth E 1992 *Relaxation and Thermodynamics in Polymers. Glass Transition* (Berlin: Akademie)

Ngai K L and Plazek D 1995 *J. Rubber Chem. Technol.* **68** 376

[2] McArdle C B (ed) 1989 *Side Chain Liquid Crystal Polymers* (Glasgow: Blackie)
[3] Xie S, Natansohn A and Rochon P 1993 *Chem. Mater.* **5** 403
Kumar G S and Neckers D C 1989 *Chem. Rev.* **89** 1915
[4] Anderle K, Birenheide R, Werner M J A and Wendorff J H 1991 *Liq. Cryst.* **5** 691
Hvilsted S, Andruzzi F, Kulinna C, Siesler H W and Ramanujam P S 1995 *Macromolecules* **28** 2172
[5] Legge C H and Mitchell G R 1992 *J. Phys. D: Appl. Phys.* **25** 492
Kanazawa A, Hirano S, Shishido A, Hasegawa M, Tsutsumi O, Shiono T, Ikeda T, Nagase Y, Akiyama E and Takamura Y 1997 *Liq. Cryst.* **23** 293
[6] Angeloni A S, Caretti D, Laus M, Chiellini E and Galli C 1991 *J. Polym. Sci.* **29** 1865
[7] Andreozzi L, Fontana M P, Francia F, Giordano M, Leporini D and Rateo M 1994 *J. Non-Cryst. Solids* **172–174** 943
[8] Clark J H 1977 *Advances in IR and Raman Spectroscopy* vol 4, ed R J H Clarke and R E Hester (London: Heyden) 109
Rotschild W 1984 *Dynamics of Molecular Liquids* (New York: Wiley)
[9] Jen S, Clark N A, Pershan P S and Priestley E B 1977 *J. Chem. Phys.* **66** 4635
[10] Kirov N, Dozov I and Fontana M P 1985 *J. Chem. Phys.* **83** 5267
[11] Fontana M P, Paris C and Polli M 1997 *Mol. Cryst. Liq. Cryst.* **304** 207
[12] Camorani P, Cristofolini L, Facci P, Fontana M P and Laus M 1999 in preparation
[13] Crane R A and Fischer G 1979 *J. Phys. D: Appl. Phys.* **12** 2019
Kremer F J B, Ringsdorf H, Schuster A, Seitz M and Weberskirch R 1996 *Thin Solid Films* **284+285** 436
[14] Andreozzi L 1997 *PhD Dissertation* University of Pisa